Relation Between Biomass Patterns and Water Flux in an Arid Drainage Basin System

Yotam Ohad Prof. Ehud Meron

July 17, 2023

Abstract

In this work we study the relations between the water flux flowing out of a drainage basin to the patterns formed by its vegetation. We find that the results agrees with previous work (Meron et al. 2004), about the relation between the vegetation patterns to the water availability gradient, and offer a way to relate the vegetation patterns to the water flux.

1 Introduction

In the study of dryland ecosystems, it was found that the basic block one needs to consider is the drainage basin (Yair et al. 1982). The drainage basin has two main components: the slope and the riverbed downhill, which is commonly a dry riverbed. The biomass ratio between the slope and the riverbed has not yet been the subject of studies addressing the effects of climate change and severe droughts on vegetation (corroborated by Prof. Moshe Shachak). This ratio depends to a large extent on the patchy nature of the vegetation that develops on the slope, which tends to self-organizes in nearly periodic patterns for nearly homogeneous slopes (Lefever et al. 1997, Valentin et al. 1999, Klausmeier 1999, Von Hardenberg et al. 2001).

A commonly observed vegetation pattern on slopped terrains is banded vegetation consisting of alternating stripes of vegetation and bare soil, oriented perpendicular to the slope direction. In this configuration each stripe benefits not only from direct rainfall but also from the interception of runoff water generated in the bare-soil stripe uphill, where the infiltration rate of surface water into the soil is lower than the rate in the vegetation stripe (Meron 2019). However, at sufficiently lower precipitation rates vegetation stripes break into arc-shaped vegetation spots and concomitantly bare-soil areas merge to form longer pathways for water flow downhill. These pathways, in turn, increase the seepage of water and nutrients from the slope to the riverbed and change the ratio of vegetation biomass between the two components. Longer pathways of water and nutrient flow are often described as increased connectivity (Okin et al. 2015)

2 The Model

2.1 Model's Equations

We will study the problem of biomass patterns in drainage basin using the model proposed by Gilad, Hardenberg, et al. 2004, and Gilad, J. von Hardenberg, et al. 2007. We choose this model as, unlike simpler models, it makes a distinction between soil water and surface water. Therefore distinguishing the surface water from the rest of the system, enabling us to examine it and water flux which derives from it.

The model can be written in a non-dimensional form as such:

$$\partial_t b = G_b(x,y)b(1-b) - b + \delta_b \nabla^2 b \tag{2.1}$$

$$\partial_t w = Ih - \nu(1-\rho b)w - G_w(x,y)w + \delta_w \nabla^2 w \tag{2.2}$$

$$\partial_t h = p - Ih - \nabla \cdot \vec{J} \tag{2.3}$$

where $b(x,y), w(x,y), h(x,y)$ are the non-dimensional functions from $\mathbb{R}^2$ to $\mathbb{R}$ describing the biomass, soil water, and surface water. $\vec{J}$ is the (non-dimensional) water flux and is given by:

$$\vec{J} = -2\delta_h h \nabla \left(h + \zeta(x,y)\right) \tag{2.4}$$

using ζ as the topography function of the slope. Assuming uniform slope $\zeta(x,y) = my$, the water flux can be written as:

$$\nabla \cdot \vec{J} = -\delta_h \nabla^2 (h^2) - 2\delta_h m \partial_y h \tag{2.5}$$

I is the infiltration rate and is defined using

$$I = \alpha \frac{b + qf}{b + q} \tag{2.6}$$

This form captures the dependence of the infiltration rate on the biomass. $f \in [0,1]$ and $q \in (0,\infty)$, so for large values of f (close to 1), the infiltration rate doesn't depends much on the biomass, while for small values of f (close to 0) the dependence is extremely large - $I \approx \alpha \frac{b}{b+q}$.

The Functions G_b, G_w are defined using the kernel function

$$g(\mathbf{x}, \mathbf{x}', t) = \frac{1}{2\pi} \exp\left[-\frac{|\mathbf{x} - \mathbf{x}'|^2}{2(1 + \eta b(\mathbf{x}, t))^2} \right] \tag{2.7}$$

as

$$G_b(\mathbf{x}, t) = \nu \int_\Omega g(\mathbf{x}, \mathbf{x}', t) w(\mathbf{x}', t) d\mathbf{x}' \tag{2.8}$$

$$G_w(\mathbf{x}, t) = \gamma \int_\Omega g(\mathbf{x}', \mathbf{x}, t) b(\mathbf{x}', t) d\mathbf{x}' \tag{2.9}$$

We add the assumption the the root zone is narrowly confined. In the dimensional form this means that $S_0 \to 0$ (see Gilad, Hardenberg, et al. 2004, eq (3)). Using this assumption we get:

$$G_b = \nu w (1 + \eta b)^2 \tag{2.10}$$

$$G_w = \gamma b (1 + \eta b)^2 \tag{2.11}$$

Our model equations are then:

$$\partial_t b = \nu b w (1 - b)(1 + \eta b)^2 - b + \delta_b \nabla^2 b \tag{2.12}$$

$$\partial_t w = Ih - \nu(1 - \rho b) w - \gamma b w (1 + \eta b)^2 + \delta_w \nabla^2 w \tag{2.13}$$

$$\partial_t h = p - Ih - \nabla \cdot \vec{J} \tag{2.14}$$

2.2 Scales of the slope

From equation 2.4, assuming uniform slope as in equation 2.1, we can write the time derivative of h in the following manner:

$$\partial_t h = \frac{1}{1 - 2\delta_h m h} \left(p - Ih + 2\delta_h h \nabla h\right) \tag{2.15}$$

From this, we can see that if $0 < 2\delta_h m h \ll 1$ then the system dynamics do not depend on the terrain's slope. This inequality will be taken into account when choosing the range of slope values to simulate over.

2.3 Uniform Bare Steady State Solution

To be able to verify that our simulation indeed represents the mathematical model correctly, we derive in this section the linear stability of the uniform bare steady state solution. This linear stability can then be checked in the simulation.

2.3.1 Solutions of the Model

The uniform bare steady state solution of the model is a solution that has no vegetation at all, and homogeneous surface and soil water. In equation form we can write this as:

$$b(x,y) = 0 \tag{2.16}$$
$$\partial_t w = \partial_t h = 0 \tag{2.17}$$
$$\nabla w = \nabla h = 0 \tag{2.18}$$

From the first condition, we can see that both $\partial_t b = 0$ and $\nabla b = 0$ holds. We are left with the following system of equations:

$$0 = \alpha h - \nu w \tag{2.19}$$
$$0 = p - \alpha f h \tag{2.20}$$

which admits the following solutions:

$$w_0 = \frac{p}{\nu} \tag{2.21}$$
$$h_0 = \frac{p}{\alpha f} \tag{2.22}$$

2.3.2 Linear Stability Analysis

We start by writing the right hand side of the model equations in operator form and equating it to zero to find the steady state.

$$\vec{0} = \vec{F}[b, w, h] \tag{2.23}$$

To find the linear stability of the uniform bare steady state solution, we'll calculate the linear approximation of $\vec{F}$ when perturbing the solution we found using $\begin{bmatrix} \varepsilon_b(t) \\ \varepsilon_w(t) \\ \varepsilon_h(t) \end{bmatrix} e^{i\vec{k}\cdot\vec{r}}$, an infinitesimal perturbations with $0 < |\varepsilon_s| \ll 1$ for $s \in \{b, w, h\}$. $\vec{r} = (x, y)$ is the position vector in the region, and $\vec{k} = (k_x, k_y)$ is the vector wave number of the perturbation ($|\vec{k}| \geq 0$).

Plugging this form into 2.23, we get the following relations:

$$\partial_t \varepsilon_b = (-\delta_b k^2 + p - 1)\varepsilon_b + o(\varepsilon^2) \tag{2.24}$$
$$\partial_t \varepsilon_w = \frac{p}{q}(1-f)\varepsilon_b + (-\delta_w k^2 - \nu)\varepsilon_w + \alpha f \varepsilon_h + o(\varepsilon^2) \tag{2.25}$$
$$\partial_t \varepsilon_h = (-\alpha - 2\delta_h \frac{p}{\alpha} k^2 + 2i\delta_h k_y m)\varepsilon_h + o(\varepsilon^2) \tag{2.26}$$

where $o(\varepsilon^2)$ are nonlinear terms in $\varepsilon_{b,w,h}$. We assume the initial perturbations are infinitesimal, we can ignore nonlinear terms in 2.24. We are left with the following linear ODE:

$$\partial_t \begin{bmatrix} \varepsilon_b \\ \varepsilon_w \\ \varepsilon_h \end{bmatrix} = \begin{bmatrix} -\delta_b k^2 + p - 1 & 0 & 0 \\ \frac{p}{q}(1-f) & -\delta_w k^2 - \nu & \alpha f \\ 0 & 0 & -\alpha - 2\delta_h \frac{p}{\alpha} k^2 + 2i\delta_h k_y m \end{bmatrix} \begin{bmatrix} \varepsilon_b \\ \varepsilon_w \\ \varepsilon_h \end{bmatrix} \tag{2.27}$$

Solutions of these equation are linear combinations of the eigenvectors of the matrix. Each eigenvector grows if its eigenvalue is positive, and decays for negative eigenvalues. Linearly stable states would have all the eigenvalues as negative. In this problem, the eigenvalues can be easily found to be:

$$\sigma_1 = -\delta_b k^2 + p - 1 \tag{2.28}$$
$$\sigma_2 = -\delta_w k^2 - \nu \tag{2.29}$$
$$\sigma_3 = -\alpha - 2\delta_h \frac{p}{\alpha} k^2 + 2i\delta_h k_y m \tag{2.30}$$

We see that the real parts of σ_2, σ_3 are negative for all $k^2 = k_x^2 + k_y^2 > 0$. For $p < 1$ we get $\sigma_1 < 0$ while for $p > 1$ there exists a range of values of k^2 for which $\sigma_1 > 0$ and the steady state loses stability. The point at which this happens is denoted p_c (critical precipitation) and can be found by solving

$$\sigma_1 = 0 \tag{2.31}$$

$$\frac{d\sigma_1}{dk} = 0 \tag{2.32}$$

The second equation gives $k = 0$ which then leads to $p = 1$. Then $p_c = 1$ (a local maximum of σ_1). For $p < 1$ then, the perturbations decrease while for $p > 1$ the perturbations grow, changing the state of the system into a non-zero biomass state. We could the p parameter in our numerical code, to check for the validity of our simulations. We note here that the slope, in the case of linear terrain, only appears in the complex part of the eigenvalues and thus doesn't effect the linear stability. Its meaning comes into play only when the system is non-homogeneous. In this case, it relates to the speed of which spatial perturbation travel up the slope.

3 Simulating the model

For the numerical simulations of the model, we used the python package `dedalus3` (Burns et al. 2020). The code used in this paper, and scripts to generate the data used, can be found at Ohad 2023.

3.1 Boundary Conditions

We now move to discuss how to simulate the model. For simplicity we choose a square region of $N \times N$ points, relating to an area of $L \times L$ we wish to simulate. For the x coordinates, we have periodic boundary conditions. For the y axis, we wish to not force the total flux coming out of the region. This leads as to consider Neumann boundary condition at the bottom edge for the flux. Using $h(x, y = 0) = h$ we can write $J_y = -2\delta_h h \frac{\partial}{\partial y}(h + \zeta)$ as the y compononent of the flux. We can then write the boundary condition as:

$$\frac{\partial J_y}{\partial y}(y = 0) = 0 \tag{3.1}$$

or in terms of h:

$$\left(\frac{\partial h}{\partial y}\right)^2 + h\frac{\partial^2 h}{\partial y^2} + m\frac{\partial h}{\partial y} = 0 \tag{3.2}$$

Using $H = \frac{\partial h}{\partial y}$ we can get a Neumann boundary condition for h, i.e., $\frac{\partial h}{\partial y} = A \in \mathbb{R}$.

$$\left(H + m + h\frac{\partial}{\partial y}\right) H = 0 \tag{3.3}$$

$$\Rightarrow \frac{1}{H(H+m)}\frac{\partial H}{\partial y} = -\frac{1}{h} \tag{3.4}$$

Integrating both sides over the range of y values we get:

$$\frac{1}{m}\ln\frac{H}{H+m} = -\int_0^{L_y}\frac{dy}{h} \tag{3.5}$$

We can isolate H

$$\frac{\partial h}{\partial y}(y = 0) = H = m\frac{e^{-m\int_0^{L_y}\frac{dy}{h}}}{1 - e^{-m\int_0^{L_y}\frac{dy}{h}}} \tag{3.6}$$

For other fields and edges in the y coordinate, we chose a zero Neumann boundary condition - $\frac{\partial f}{\partial y} = 0$. Note that this additional condition makes the flux at the top edge equals to mh. This means our top edge isn't the separation line between drainage basins.

3.2 Results

The values of the constants of the non-dimensional model were taken from (Gilad, J. von Hardenberg, et al. 2007). The values used are shown in Table 1.

constant	value
m	$[0, 10]$
p	$[0.9, 1.5]$
ν	$\frac{10}{3}$
η	3.5
ρ	0.95
γ	$\frac{50}{3}$
α	0.1
q	0.05
f	0.01
δ_b	$\frac{1}{30}$
δ_w	$\frac{10}{3}$
δ_h	$\frac{1}{300}$

Table 1: Values of simulation's constants.

First, we checked that the numerical simulation indeed reproduces the linear stability analysis. The simulation started from the homogeneous non-bare state, and was left to run for 500 years. The precipitation values where chosen to be around p_c (the critical precipitation). Figure 1 shows the results of the simulation. We see that for $p < p_c$ the system decays to the zero state, while for $p > p_c$ the system moves to a nonzero state. This is in agreement with the linear stability analysis. Below p_c the perturbations decay, while above p_c they grow.

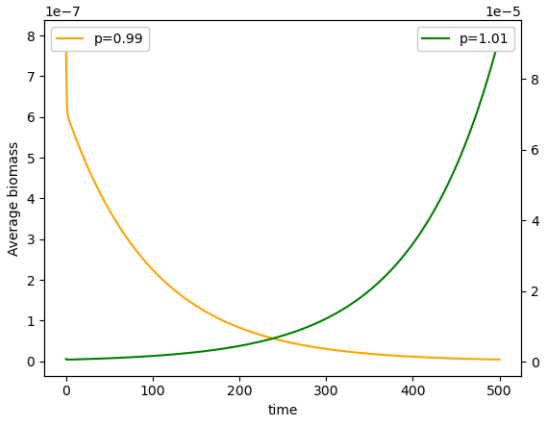

Figure 1: Simulations around p_c (different scales)

We now move to study the water flux in the system in the case of $p > p_c$. We started each simulation from the nonzero uniform state, where the precipitation was chosen to be lower than the stationary state precipitation. We let the simulation run for 500 years, and plotted the flux going out of the region. We simulated different slopes (figure 2) and different precipitation values (figure 3).

Figure 2: Flux out of the region for various values of m.

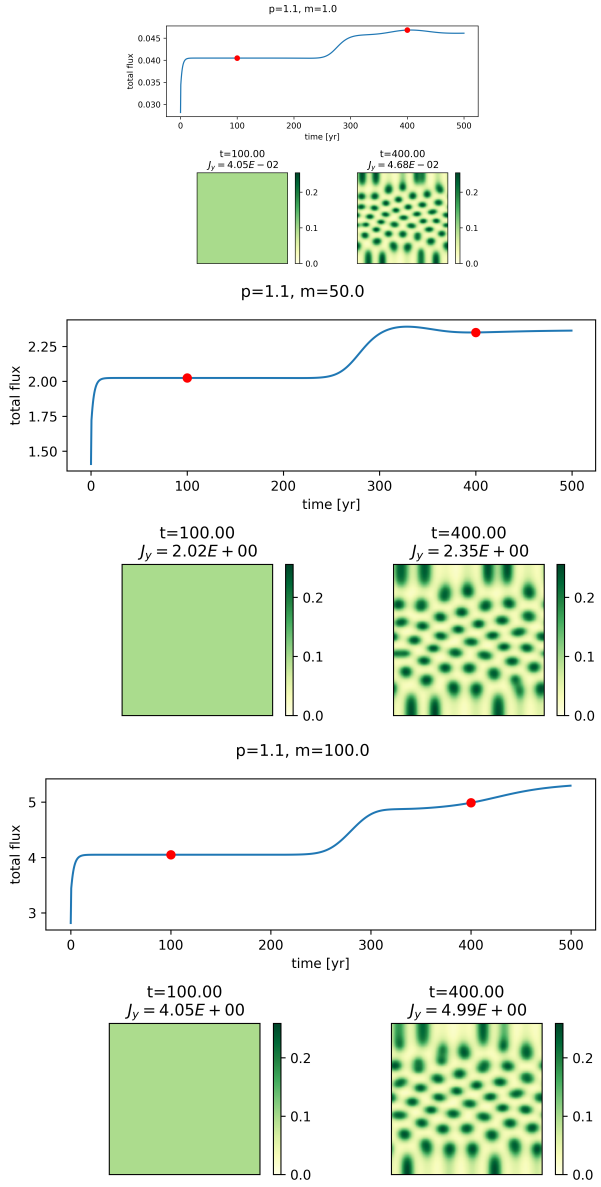

4 Discussion

Figure 1 Shows that p_c is the critical precipitation in the numerical simulation. Furthermore, The first mode to grow in the simulations is the nonzero uniform state, which is related to the dispersion curve 2.28, where the first mode to grow is the uniform mode, $k = 0$. Those phenomena where anticipated by the model, and assure us that our numerical simulation is correct.

In figure 3 we see the expected result, that as we increase the precipitation, the final pattern in the simulation is higher in the rainfall gradient. Furthermore, we can see the higher the precipitation, the lower the outward flux. This suggest that higher patterns in the rainfall gradient are more efficient in absorbing water. We explain the increased outward water flux to a higher degree of water connectivity in the hexagonal spots, and in a lesser extent stipes and holes. That is to say, water can move farther without being absorbed

Figure 3: Flux out of the region for various values of p.

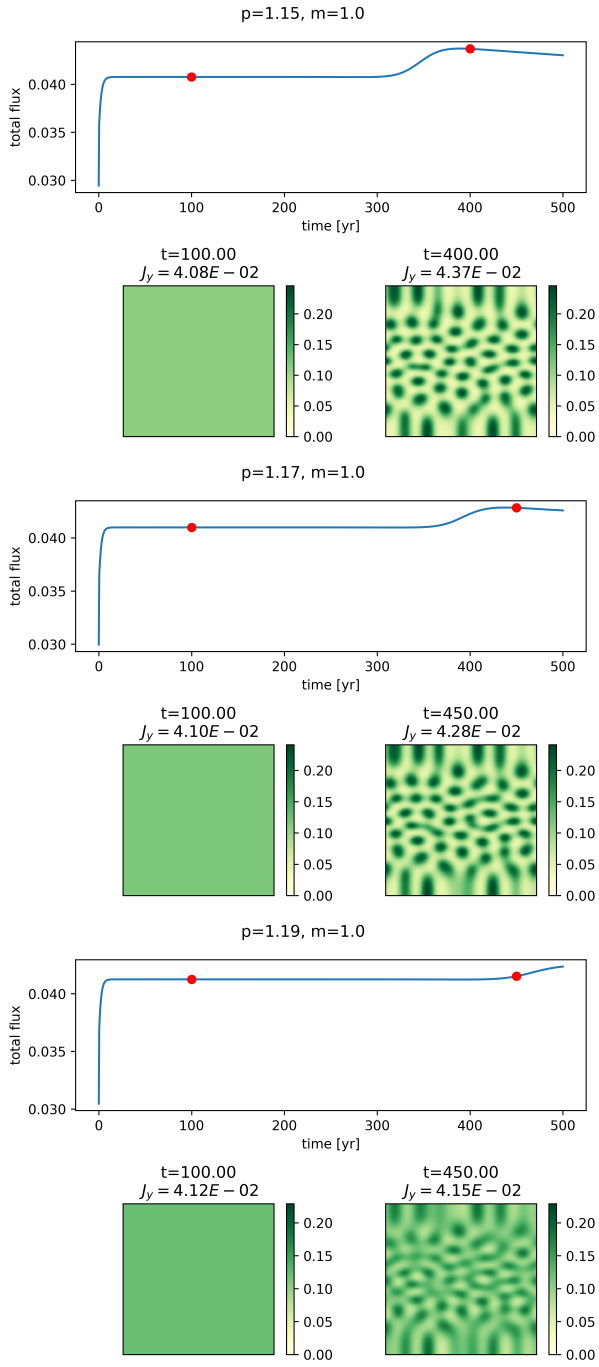

by the soil or vegetation.

Increasing the slope in the simulations (figure 2) yields different results than increasing the precipitation. We see that the higher the slope, the less stable the new outwardflux is, after the transition from the uniform nonzero state. While the overall dynamics of the system, uniform nonzero state to hexagonal pattern, remains the same. This suggest that the slope doesn't effect the system dynamics, but does effect the outward flux.

In areas that goes through droughts or desertification, precipitation becomes lower. We see from our simulations that this can be a cause to the higher rate of floods occuring in such area. The lower precipitation causes the system to move to a lower pattern in the rainfall gradient, which in turn causes a higher connectivity in the surface water. This higher connectivity apears as increased floods.

5 Bibliography

References

Burns, Keaton J. et al. (Apr. 2020). "Dedalus: A flexible framework for numerical simulations with spectral methods". In: *Physical Review Research* 2.2, 023068, p. 023068. DOI: 10.1103/PhysRevResearch.2.023068. arXiv: 1905.10388 [astro-ph.IM].

Gilad, E., J Hardenberg, et al. (2004). *Phys. Rev. Lett. 93, 098105 (2004) - Ecosystem Engineers: From Pattern Formation to Habitat Creation*. URL: https://journals-aps-org.elib.openu.ac.il/prl/abstract/10.1103/PhysRevLett.93.098105 (visited on 03/05/2023).

Gilad, E., J. von Hardenberg, et al. (Feb. 21, 2007). "A mathematical model of plants as ecosystem engineers". In: *Journal of Theoretical Biology* 244.4, pp. 680–691. ISSN: 0022-5193. DOI: 10.1016/j.jtbi.2006.08.006. URL: https://www.sciencedirect.com/science/article/pii/S0022519306003493 (visited on 03/05/2023).

Klausmeier, Christopher A. (June 11, 1999). "Regular and Irregular Patterns in Semiarid Vegetation". In: *Science* 284.5421, pp. 1826–1828. ISSN: 0036-8075, 1095-9203. DOI: 10.1126/science.284.5421.1826. URL: https://www.science.org/doi/10.1126/science.284.5421.1826 (visited on 05/24/2023).

Lefever, R et al. (1997). "On the origin of tiger bush". In.

Meron, Ehud (Nov. 1, 2019). "Vegetation pattern formation: The mechanisms behind the forms". In: *Physics Today* 72.11, pp. 30–36. ISSN: 0031-9228, 1945-0699. DOI: 10.1063/PT.3.4340. URL: http://physicstoday.scitation.org/doi/10.1063/PT.3.4340 (visited on 05/24/2023).

Meron, Ehud et al. (Jan. 2004). "Vegetation patterns along a rainfall gradient". In: *Chaos, Solitons & Fractals* 19.2, pp. 367–376. ISSN: 09600779. DOI: 10.1016/S0960-0779(03)00049-3. URL: https://linkinghub.elsevier.com/retrieve/pii/S0960077903000493 (visited on 05/24/2023).

Ohad, Yotam (June 2023). *Relation Between Biomass Patterns and Water Flux*. Version 1.0.0. URL: https://github.com/yohad/water-connectivity.

Okin, Gregory S et al. (2015). "Connectivity in dryland landscapes: shifting concepts of spatial interactions". In: *Frontiers in Ecology and the Environment* 13.1. _eprint: https://esajournals.onlinelibrary.wiley.com/doi/pdf/10.1890/14 pp. 20–27. ISSN: 1540-9309. DOI: 10.1890/140163. URL: https://onlinelibrary.wiley.com/doi/abs/10.1890/140163 (visited on 05/24/2023).

Valentin, C et al. (Sept. 1999). "Soil and water components of banded vegetation patterns". In: *CATENA* 37.1, pp. 1–24. ISSN: 03418162. DOI: 10.1016/S0341-8162(99)00053-3. URL: https://linkinghub.elsevier.com/retrieve/pii/S0341816299000533 (visited on 05/24/2023).

Von Hardenberg, J. et al. (Oct. 18, 2001). "Diversity of Vegetation Patterns and Desertification". In: *Physical Review Letters* 87.19, p. 198101. ISSN: 0031-9007, 1079-7114. DOI: 10.1103/PhysRevLett.87.198101. URL: https://link.aps.org/doi/10.1103/PhysRevLett.87.198101 (visited on 05/24/2023).

Yair, A. et al. (Sept. 1982). "A case study of energy, water and soil flow chains in an arid ecosystem". In: *Oecologia* 54.3, pp. 389–397. ISSN: 0029-8549, 1432-1939. DOI: 10.1007/BF00380008. URL: http://link.springer.com/10.1007/BF00380008 (visited on 05/24/2023).